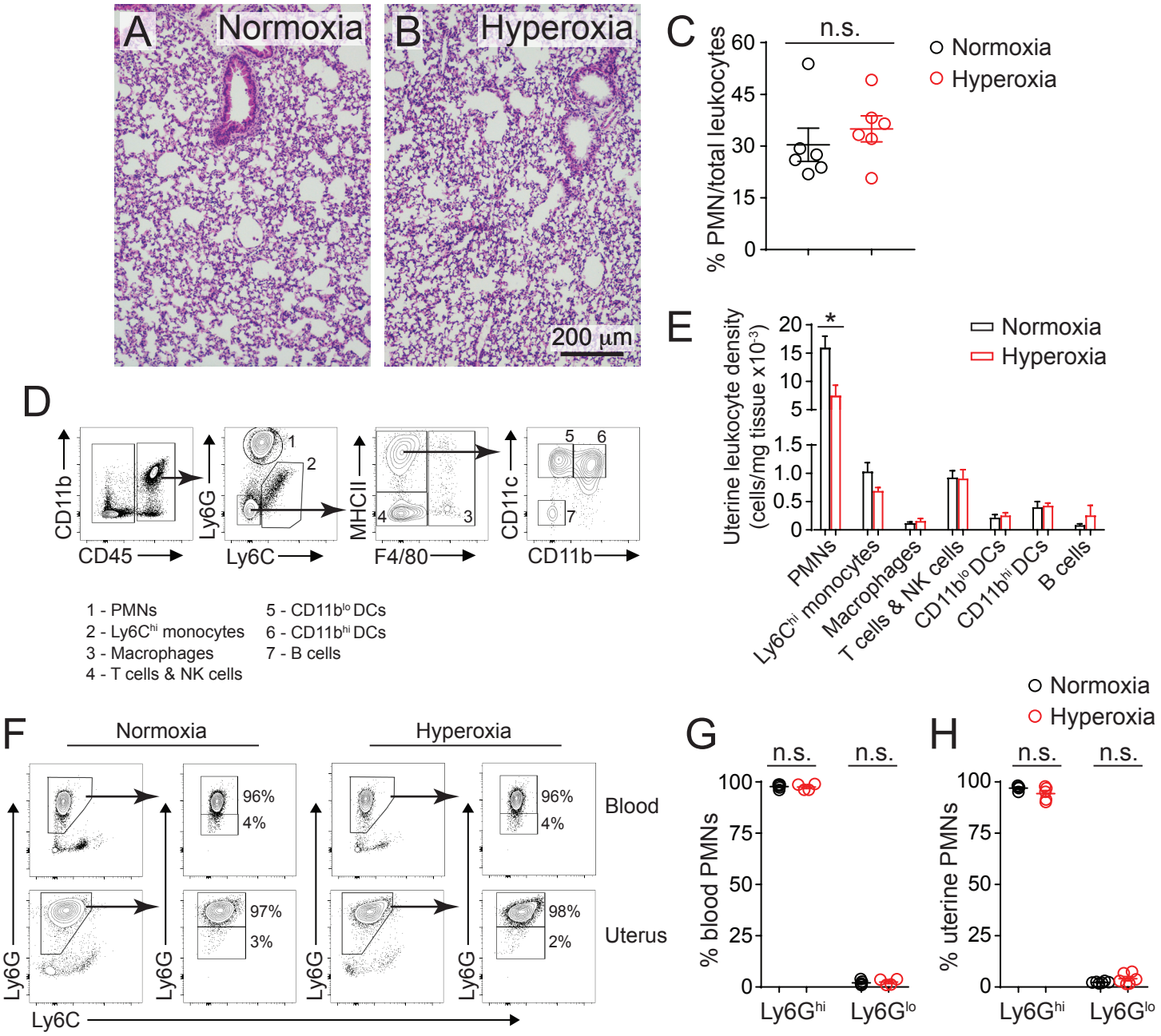

Supplemental Figure 1. Characteristics of lungs, blood and uteri of PRPL mice housed in normoxia or hyperoxia conditions. Mice were housed in either ambient O_2 (normoxia conditions) or 60% O_2 (hyperoxia conditions) for the last 10 days prior to sacrifice on P28. (A, B) Representative H&E-stained lung sections (n=6 mice/group). (C) PMN frequencies in the lung. The graph also shows mean±SEM. n.s., not significant by two-tailed Mann-Whitney U test. PMNs were identified through a gating strategy akin to that shown in panel D. (D) Flow cytometric gating strategy to identify uterine leukocyte subsets. The cells were first gated for doublet discrimination and dead cell exclusion. The Ly6C antibody was conjugated to AF700 so its absolute staining intensity was low. The cells indicated as Ly6C^{hi} monocytes stain brightly for Ly6C when other fluorochromes are used. T and NK cells in this experiment were identified by exclusion; separate staining panels revealed that his gate contained ~46% TCRβ$^+$ T cells, ~18% TCRδ$^+$ T cells, and ~33% NK1.1$^+$ NK cells. (E) Uterine leukocyte tissue densities (mean±SEM, n=6 mice per group; *, P<0.05 by two-tailed Mann-Whitney U test). The PMN data are the same as in Figure 1A. No significant differences were detected between housing conditions for the other subsets. (F) Representative flow cytometry plots (n=4-7 mice/group) and (G, H) quantification of Ly6G expression by blood and uterine PMNs, to assess PMN maturation status. The plots were initially gated on all viable CD45$^+$ CD11b$^+$ cells. The graphs also show mean±SEM. n.s., not significant by two-tailed Mann-Whitney U test.

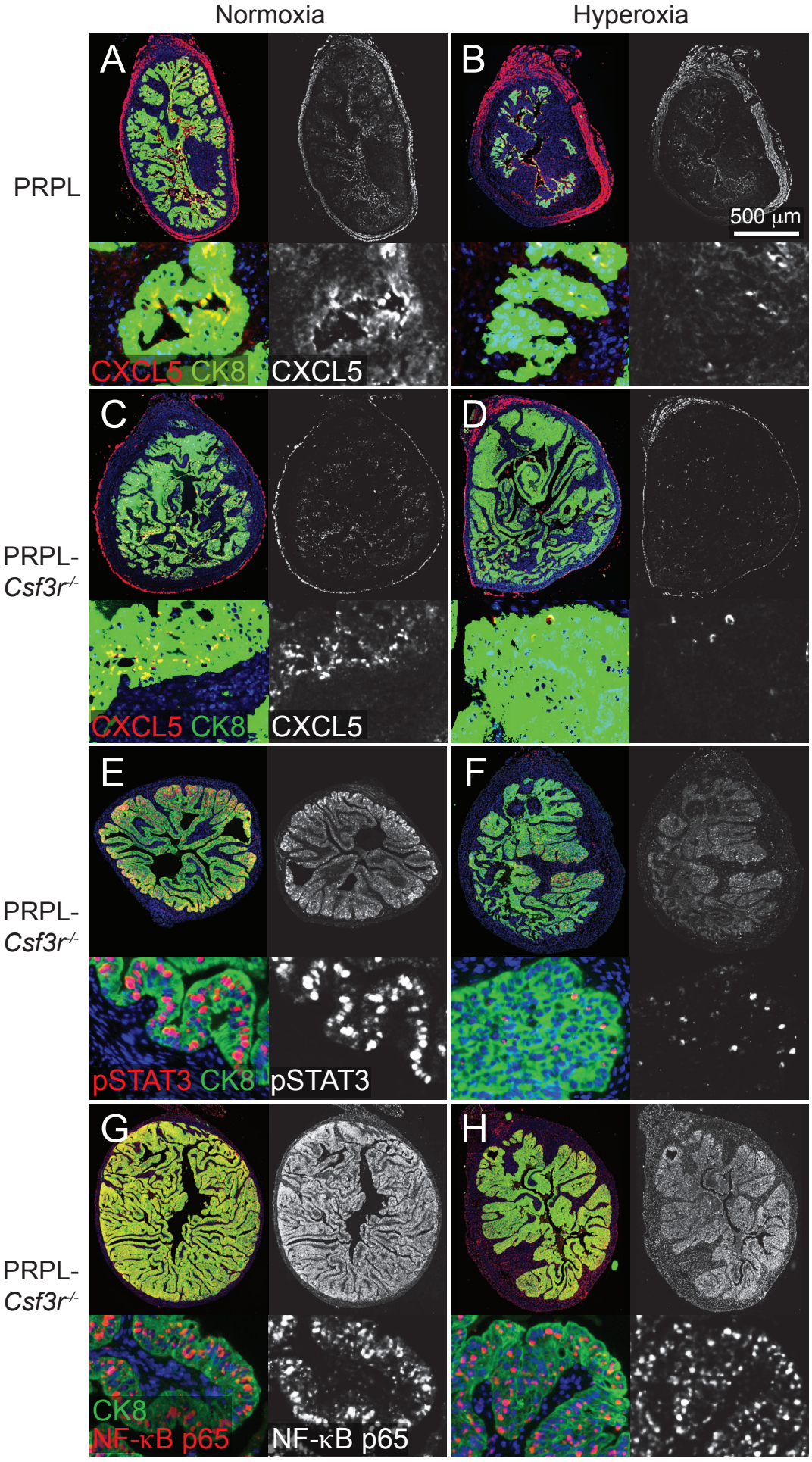
Normoxia
Hyperoxia
PRPL
PRPL-
Csf3r-/-
PRPL-
Csf3r-/-
PRPL-
Csf3r-/-
A
B
C
D
E
F
G
H
500 μm
CXCL5 CK8
CXCL5
CXCL5 CK8
CXCL5
pSTAT3 CK8
pSTAT3
CK8
NF-κB p65
NF-κB p65

Supplemental Figure 2. Further effects of hyperoxia housing on PRPL and PRPL-*Csf3r*$^{-/-}$ uteri. Sections were stained with the indicated antibodies and representative images from *n*=6 mice per group are shown. Lower panels show close-ups, with DAPI counterstain in the color images. The display of the CK8 co-stain was manipulated in order to best reveal the salient staining characteristics of the other antibody. Thus, for CXCL5 immunostaining (A-D), whose pattern was non-nuclear, we set a low threshold for CK8 so that the nuclear spaces would be less overt. Conversely, for pSTAT3 (E, F), NF-κB p65 (G, H), and HIF-1α (Figure 1E and F), we set a higher CK8 threshold to reveal the nuclear spaces. The CXCL5 staining in the myometrium appeared artifactual as it was not cell-associated.

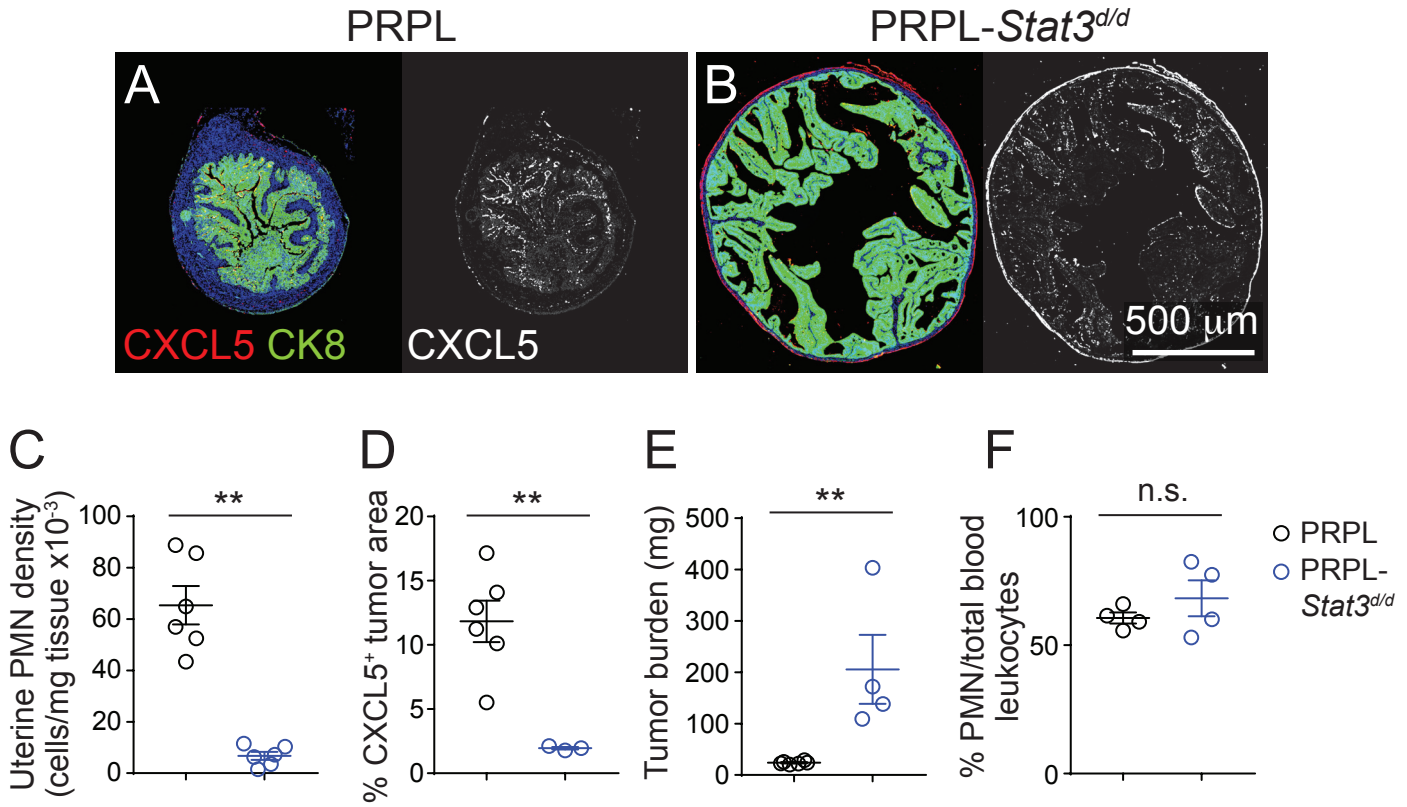

Supplemental Figure 3. STAT3 is required for CXCL5 expression by tumor cells and PMN recruitment to the PRPL uterus. To assess the role of STAT3 signaling in PRPL tumorigenesis, we generated *Pgr*-Cre *Pten*$^{lox/lox}$ *Stat3*$^{lox/lox}$ mice (i.e. PRPL-*Stat3*$^{d/d}$ mice), to direct uterus-specific STAT3 deletion superimposed upon uterus-specific *Pten* deletion. The mice were sacrificed on P28. (A, B) Representative double CXCL5/CK8 immunofluorescence images (n=3-6 mice/group). The CXCL5 staining in the myometrium appeared artifactual as it was not cell-associated. (C) Uterine PMN densities, as determined by flow cytometry. (D, E) Quantification of (D) tumor cell CXCL5 expression and (E) tumor burden, determined as in Figures 1C and 2A, respectively. (F) PMN frequencies in the blood. Uterine PMN densities, tumor burdens and blood PMN frequencies were determined using a cohort of PRPL mice distinct from the cohort analyzed throughout the rest of the study but sacrificed at the same time as the PRPL-*Stat3*$^{d/d}$ mice. The CXCL5 staining data for PRPL mice is the same as in Figure 1C. Together, this analysis thus revealed that, at 4 wks of age, PRPL-*Stat3*$^{d/d}$ mice had a much greater tumor burden than PRPL mice (E), an almost complete loss of uterine PMNs (C), and a maintenance of the papillary tumor morphology (B) that in PRPL mice is lost after 3 wks of age when PMNs start infiltrating into the uterus (see ref. (5) for a discussion of this shift in tumor morphology). In these respects, PRPL-*Stat3*$^{d/d}$ mice phenocopied PMN-deficient PRPL-*Csf3r*$^{-/-}$ mice. Moreover, PRPL-*Stat3*$^{d/d}$ mice showed a virtually complete loss of CXCL5 expression by tumor cells (D), which together with their unchanged PMN numbers in the blood compared to PRPL mice (F), suggested a major impairment of PMN recruitment to the uterus. Thus, together with our findings that hyperoxia housing decreased pSTAT3 expression by PRPL tumor cells (Figure 1D, Supplemental Figure 2E-F), these data suggest a scenario in which hypoxia induces pSTAT3 activation in PRPL tumor cells, to in turn induce their expression of CXCL5 (and possibly CXCL1 and CXCL2, the two other CXCR2 ligands in mice) and thus PMN recruitment to the uterus. pSTAT3 staining in the uterine epithelium of PRPL-*Stat3*$^{d/d}$ mice was completely absent, as expected (not shown). **, P<0.01 by two-tailed Mann-Whitney U test; n.s., not significant.

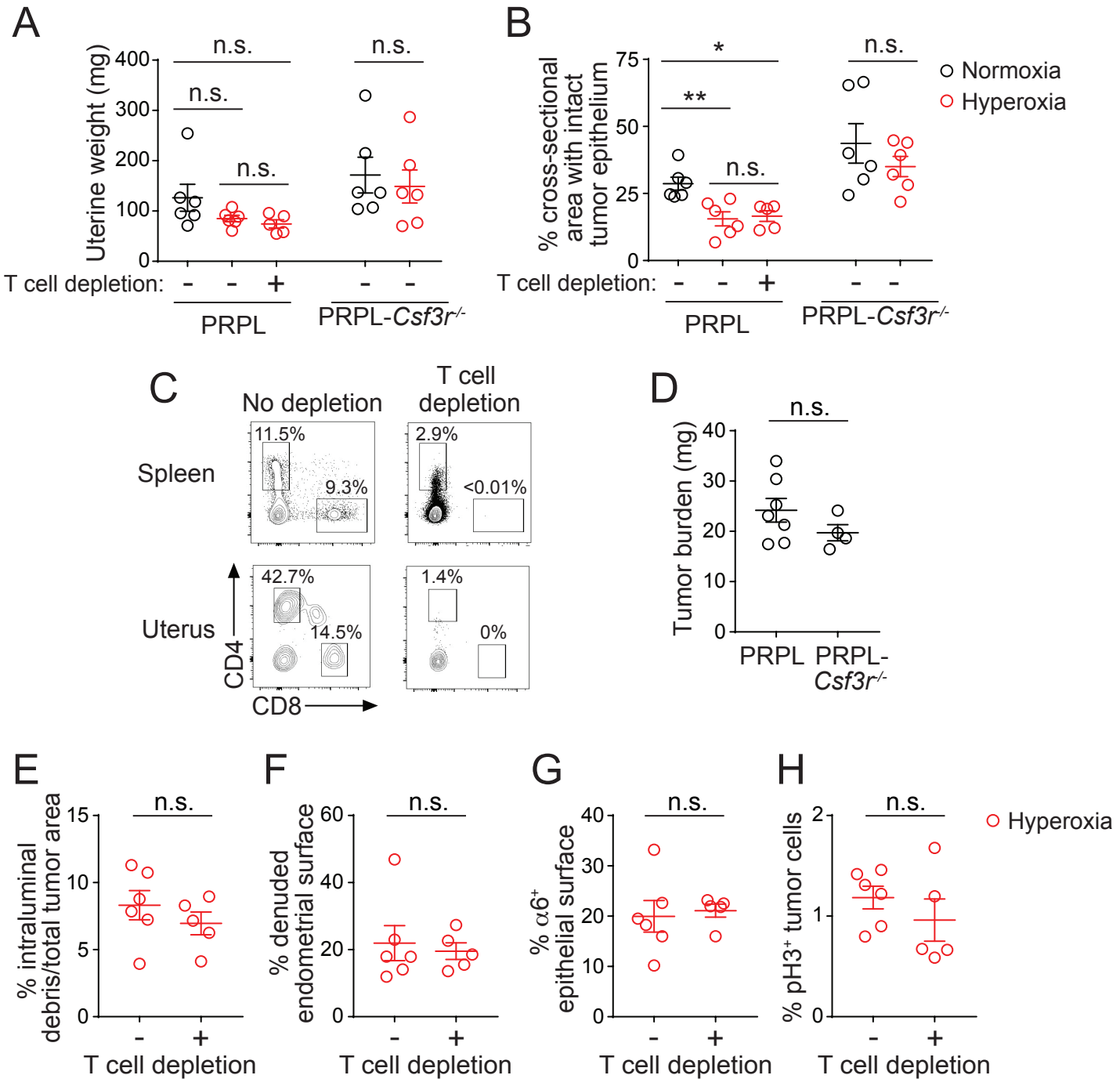

Supplemental Figure 4. Additional analysis of hyperoxia-housed mice. (A) Uterine weights and (B) percent cross-sectional uterine area occupied by an intact (i.e., non-sloughed) E-Cad$^+$ tumor epithelium, averaged from 3-5 sections per mouse. For each mouse, these two quantities were multiplied together to calculate the tumor burdens shown in Figure 2. Graphs also show mean±SEM. *, P<0.05; **, P<0.01 by two-tailed Mann-Whitney U test; n.s., not significant. Data for PRPL mice were first assessed by the Kruskal-Wallis test (P<0.001) and P-values were Bonferroni-adjusted for multiple comparisons. (C) Representative flow cytometric analysis (n=5-6 mice per group) of spleens (live/CD45$^+$/Ly6G$^-$ gating) and uteri (live/CD45$^+$/Ly6G$^-$/CD90.2$^+$ gating) from hyperoxia-housed PRPL mice treated with or without T cell-depleting antibodies. (D) Tumor burden on P18, calculated as the product of uterine weight and percent cross-sectional area of uterus comprised of tumor cells. Tumor cells were identified by E-Cad immunostaining. (E-H) Effect of T cell depletion on various sub-parameters of tumor growth in PRPL mice housed under hyperoxia conditions. Data for hyperoxia-housed, but otherwise untreated PRPL mice are the same as in Figure 3G-J. Graphs in D-H also show mean±SEM and data were analyzed by two-tailed Mann-Whitney U test; n.s., not significant.

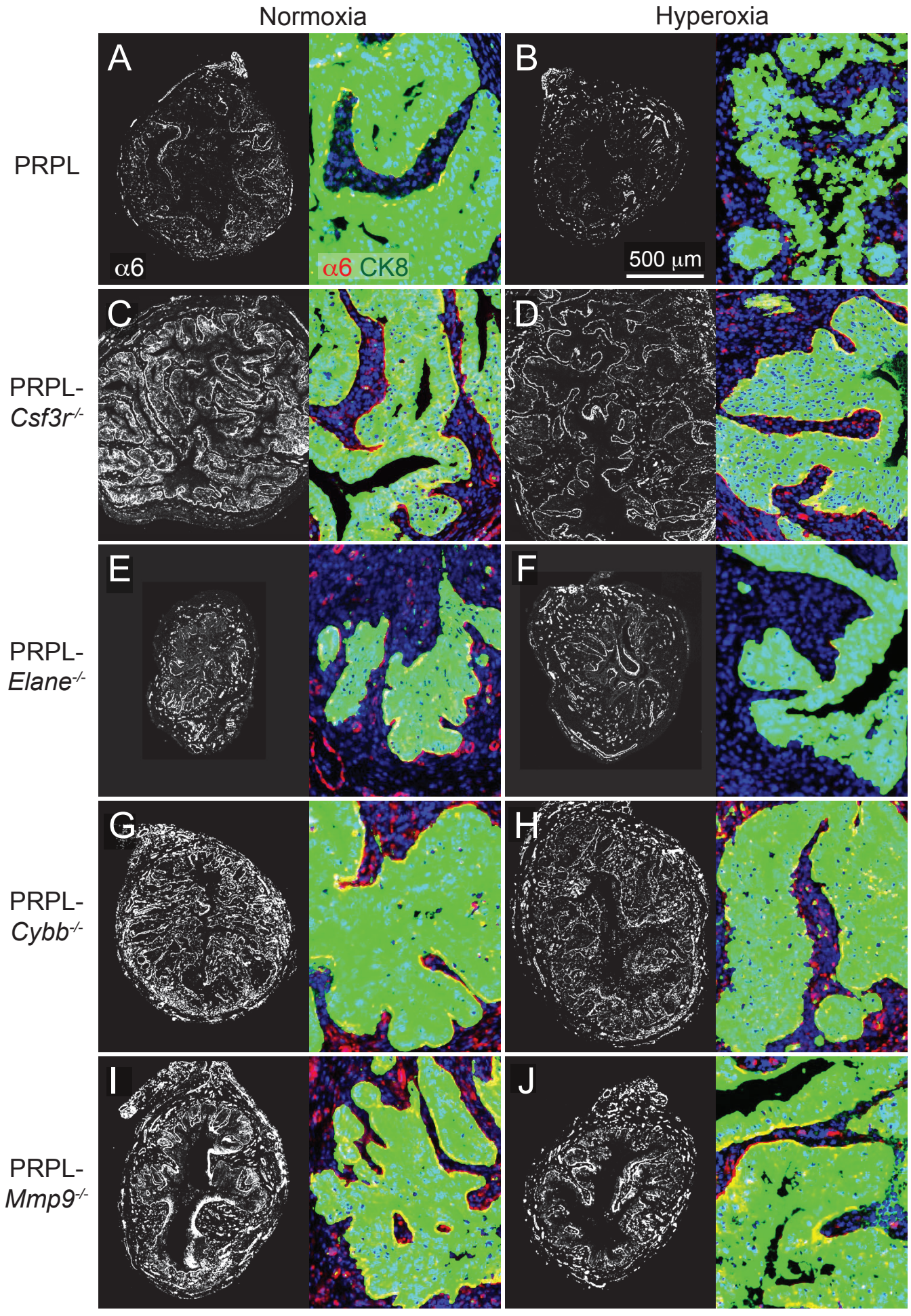
Normoxia
Hyperoxia
PRPL
PRPL-
Csf3r-/-
PRPL-
Elane-/-
PRPL-
Cybb-/-
PRPL-
Mmp9-/-
A
B
C
D
E
F
G
H
I
J
α6
α6 CK8
500 μm

Supplemental Figure 5. Effects of hyperoxia and *Elane*, *Cybb*, and *Mmp9* deficiencies on integrin α6 distributions. Representative images of α6 integrin immunofluorescence (*n*=6 mice/group), with close-ups also showing CK8 and DAPI counterstains. Note the discontinuous pattern of α6 staining along the basolateral tumor surface for PRPL and PRPL-*Elane*$^{-/-}$ mice but the largely continuous pattern for PRPL-*Csf3r*$^{-/-}$, PRPL-*Cybb*$^{-/-}$ and PRPL-*Mmp9*$^{-/-}$ mice. Vascular structures are also α6^{+}.

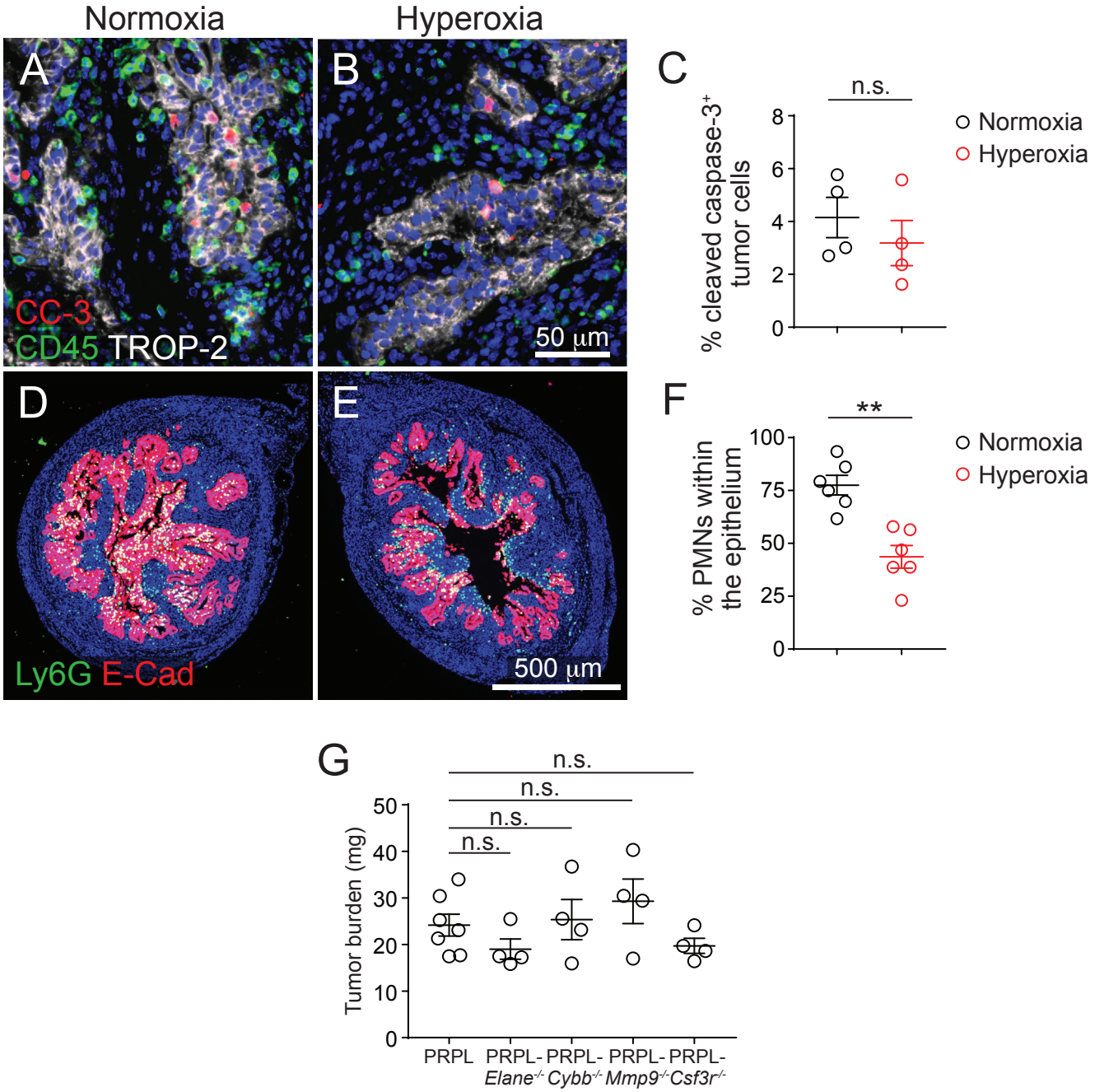

Supplemental Figure 6. Effects of respiratory hyperoxia on tumor cell apoptosis and uterine PMN distributions, and further effects of *Elane*, *Cybb*, and *Mmp9* deficiencies on PRPL tumor growth. (A, B) Representative cleaved caspase-3(CC-3)/CD45/TROP-2 immunostaining (n=4 mice/group) to identify apoptotic tumor cells. TROP-2 was used as an epithelial marker in this experiment to facilitate the triple staining. (C) Quantification of apoptotic tumor cell (CC-3$^+$ TROP-2$^+$ CD45$^-$) frequencies (mean±SEM; n.s., not significant by two-tailed Mann-Whitney U test). (D, E) Representative Ly6G/E-Cad-stained uterine sections of PRPL mice housed under normoxia and hyperoxia conditions (n=6 mice/group). (F) Quantification of PMN positioning within the uterine stroma versus epithelium of PRPL mice (mean±SEM; **, P <0.01 by two-tailed Mann-Whitney U test). (G) Tumor burden on P18, calculated as the product of uterine weight and percent cross-sectional area of uterus comprised of tumor cells. Tumor cells were identified by E-Cad-immunostaining (mean±SEM; all mutants were compared to PRPL by two-tailed Mann-Whitney U test; n.s., not significant). PRPL data are the same as shown in Supplemental Figure 4D.

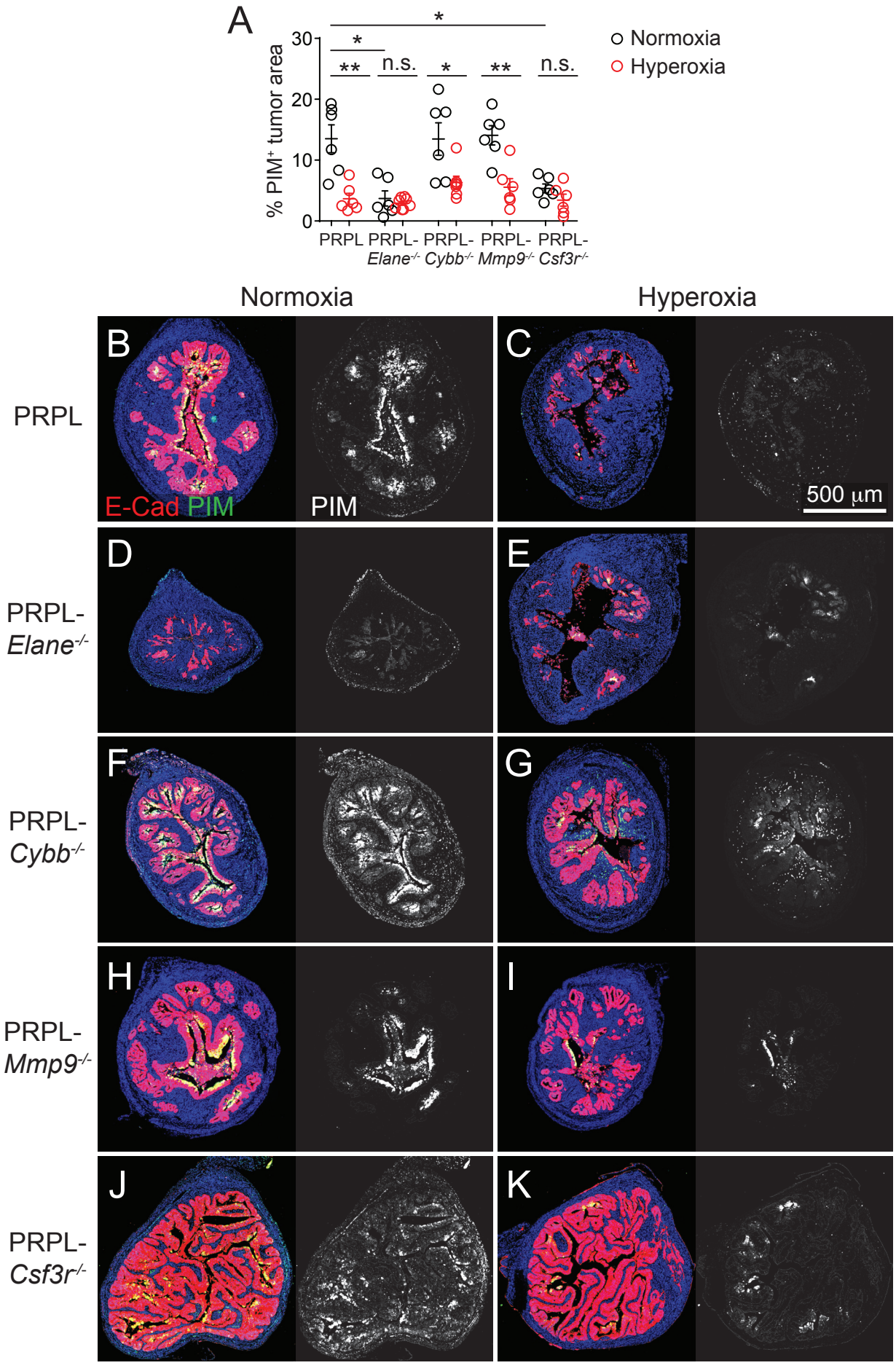
A
% PIM+ tumor area
30
20
10
0
*
*
**
n.s.
*
**
n.s.
Normoxia
Hyperoxia
PRPL
PRPL-Elane-/-
PRPL-Cybb-/-
PRPL-Mmp9-/-
PRPL-Csf3r-/-
Normoxia
Hyperoxia
B
C
D
E
F
G
H
I
J
K
PRPL
PRPL-Elane-/-
PRPL-Cybb-/-
PRPL-Mmp9-/-
PRPL-Csf3r-/-
E-Cad PIM
PIM
500 μm

Supplemental Figure 7. Effects of *Elane*, *Cybb*, and *Mmp9* deficiencies on degrees of severe tumor hypoxia. (A) Quantification of pimonidazole (PIM) uptake by tumor cells. PIM was injected 1.5 h prior to sacrifice on P28. The cross-sectional area of tumor cells positive for PIM was determined by immunofluorescence staining of uterine tissue sections and normalized to the cross-sectional area of all tumor cells, as identified by E-Cad co-staining. The graph also shows mean±SEM. *, P <0.05; **, P <0.01 by two-tailed Mann-Whitney U test; n.s., not significant. Differences between normoxia-housed mice were first assessed by the Kruskal-Wallis test (P<0.05) and P-values were Bonferroni-adjusted for multiple comparisons. (B-K) Representative images.

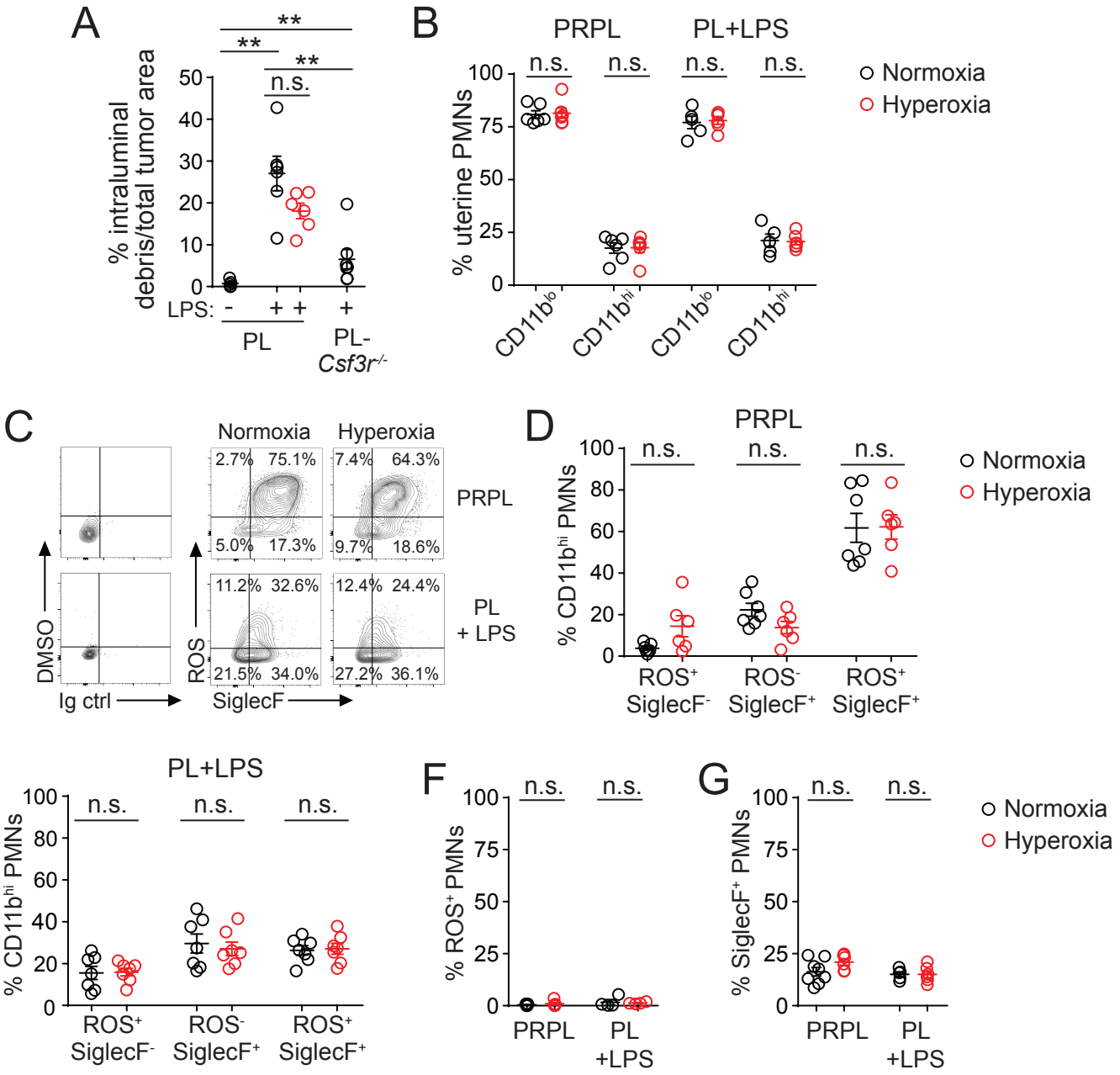

Supplemental Figure 8. Further characterization of PMNs in PRPL and LPS-injected PL mice housed in normoxia and hyperoxia conditions. PL mice were given intrauterine LPS injections 24 h prior to sacrifice. (A) Quantification of tumor cell sloughing, determined using E-Cad-stained sections. Differences between normoxia-housed mice were first assessed by the Kruskal-Wallis test ($P<0.0001$) and P-values were Bonferroni-adjusted for multiple comparisons. (B) Percentages of $CD11b^{lo}$ and $CD11b^{hi}$ PMNs in the blood and uteri of PRPL and LPS-injected PL mice, as determined by flow cytometry (see Figure 6D for gating). (C-E) Representative flow cytometry plots (C) and quantification (D, E) of ROS production and SiglecF expression by uterine $CD11b^{hi}$ PMNs (n=6-7 mice/group). DMSO is the solvent for the ROS detection reagent. (F, G) Flow cytometric quantification of ROS production and SiglecF expression by total blood PMNs (i.e. no CD11b discrimination). Graphs also show mean±SEM. **, $P<0.01$ by two-tailed Mann-Whitney U test; n.s., not significant.

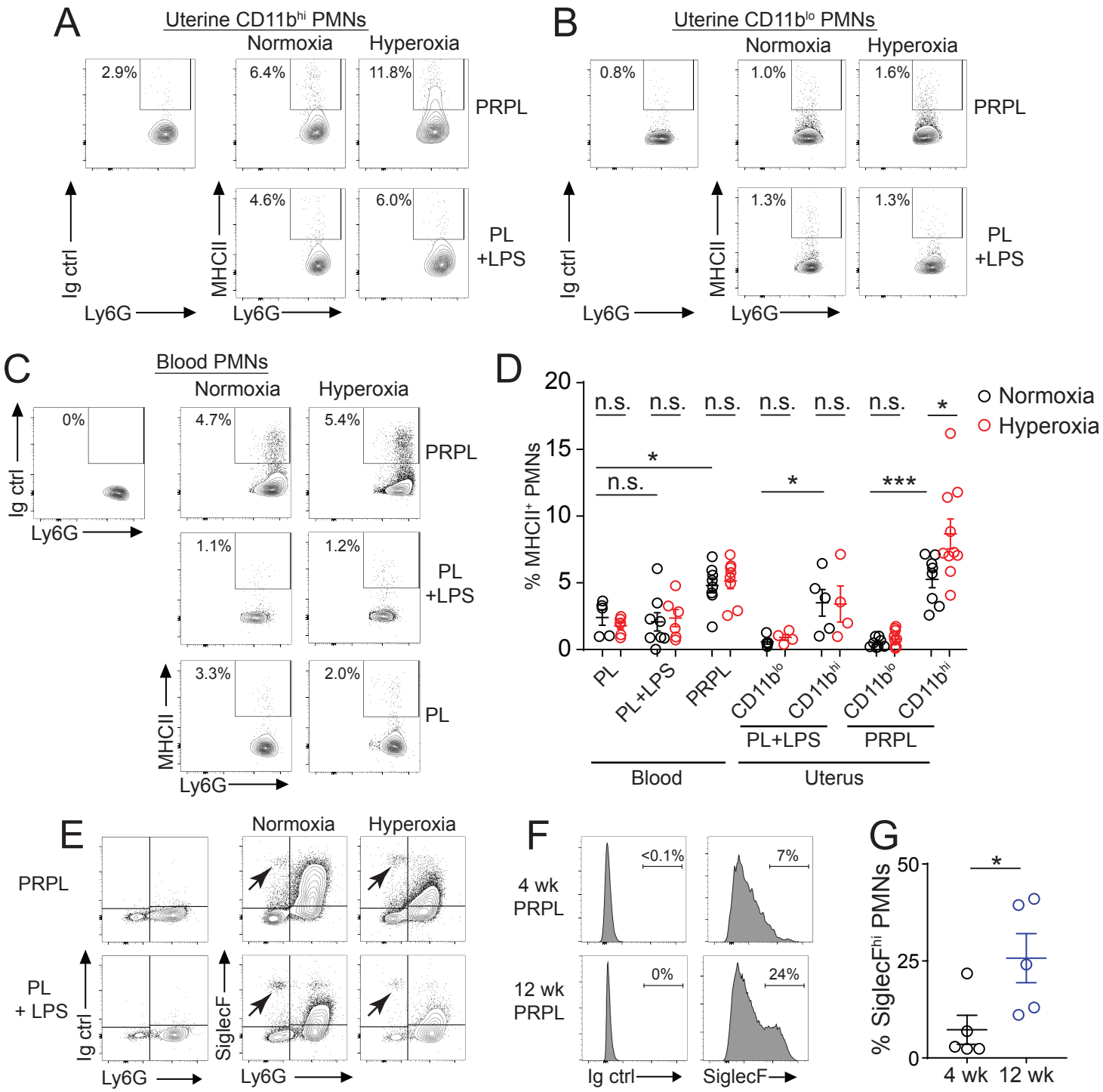

Supplemental Figure 9. MHCII and SiglecF expression by PMNs in PRPL and LPS-injected mice. (A-C) Representative flow cytometry plots showing MHC class II expression by uterine (A, B) and blood (C) PMNs. The plots were gated on live/CD45$^+$/Ly6G^{hi} events, and then subdivided, for the uterine cells, according to CD11b expression. (D) Quantification of MHC class II expression. The graph also shows mean±SEM. *, P <0.05; ***, P <0.001 by two-tailed Mann-Whitney U test; n.s., not significant. Differences between blood samples from normoxia-housed mice were first assessed by the Kruskal-Wallis test (P<0.05) and P-values were Bonferroni-adjusted for multiple comparisons. (E) Representative flow cytometry plots comparing SiglecF expression by PMNs to eosinophils (Ly6G$^-$ SiglecF^{hi} cells; arrows) in 4-wk old mice. The plots were gated on live/CD45$^+$ events. Note that only a small fraction of uterine SiglecF$^+$ PMNs in PRPL mice expressed SiglecF at the level of eosinophils and that these cells did not form a discrete population. (F, G) Representative histograms (F) and quantification (G) of the percentage of uterine PMNs with SiglecF^{hi} expression at different stages of PRPL tumor development. The histograms were gated on live/Ly6G$^+$ events and show the marker for Ly6G^{hi} expression. The graph also shows mean±SEM. *, P <0.05 by two-tailed Mann-Whitney U test.